Sub-barrier radioactive ion beam investigations using a new methodology and analysis for the stacked target technique

M. Fisichella,[1,*] A. C. Shotter,[2] A. Di Pietro,[1] P. Figuera,[1] M. Lattuada,[1,3] C. Marchetta,[1] V. Privitera,[4] L. Romano,[3,4] C. Ruiz,[5] and M. Zadro[6]

[1]*INFN, Laboratori Nazionali del Sud, via S. Sofia 62, I-95123 Catania, Italy*

[2]*School of Physics and Astronomy, University of Edinburgh, JCMB, Mayfield Road, Edinburgh EH9 3JZ, United Kingdom*

[3]*Dipartimento di Fisica ed Astronomia, via S. Sofia 64, I-95125 Catania, Italy*

[4]*CNR-IMM MATIS, via S. Sofia 64, Catania, Italy*

[5]*TRIUMF 4004 Wesbrook Mall Vancouver BC V6T 2A3, Canada*

[6]*Ruđjer Bošković Institute, Bijenička cesta 54, HR-10000 Zagreb, Croatia*

(Received 3 July 2015; published 28 December 2015)

For low energy reaction studies involving radioactive ion beams, the experimental reaction yields are generally small due to the low intensity of the beams. For this reason, the stacked target technique has been often used to measure excitation functions. This technique offers considerable advantages since the reaction cross-section at several energies can be simultaneously measured. In a further effort to increase yields, thick targets are also employed. The main disadvantage of the method is the degradation of the beam quality as it passes through the stack due to the statistical nature of energy loss processes and any nonuniformity of the stacked targets. This degradation can lead to ambiguities of associating effective beam energies to reaction product yields for the targets within the stack and, as a consequence, to an error in the determination of the excitation function for the reaction under study. A thorough investigation of these ambiguities is reported, and a best practice procedure of analyzing data obtained using the stacked target technique with radioactive ion beams is recommended. Using this procedure a re-evaluation is reported of some previously published sub-barrier fusion data in order to demonstrate the possibility of misinterpretations of derived excitation functions. In addition, this best practice procedure has been used to evaluate, from a new data set, the sub-barrier fusion excitation function for the reaction ^{6}Li + ^{120}Sn.

DOI: 10.1103/PhysRevC.92.064611 PACS number(s): 25.60.Pj, 25.70.Jj, 25.70.Gh

I. INTRODUCTION

A. Radioactive beam experiments

In the past few decades, with the availability of radioactive ion beams (RIBs), a lot of effort has been devoted to experimental investigations of collisions induced by halo and/or weakly bound nuclei. It is expected that the very low breakup threshold of such nuclei combined with the halo or cluster structure of the ground state can strongly affect the reaction dynamics around the Coulomb barrier (e.g., Refs. [1–3]). In fact, for such nuclei, direct reaction processes such as breakup or transfer can be favored by the low breakup threshold coupled with the cluster or halo structure. In addition, since the continuum of such nuclei is very close to the ground state, coupling to continuum effects become important both for elastic and for the different reaction channels, and a complete theoretical description of such collisions requires complex continuum discretized coupled channels (CDCC) calculations (e.g., Refs. [4–6]). As an example, fusion excitation functions induced by such nuclei may be affected by static and dynamic effects. Static effects are due to the fact that the diffuse surface of these nuclei affects the shape of the projectile-target potential, reducing the average Coulomb barrier, thus leading to a possible enhancement of the fusion cross-section. New dynamic effects on fusion due to coupling to the continuum have also to be taken account of. Moreover, fusion reactions in collisions induced by halo or weakly bound nuclei on light or medium mass targets are complicated by the fact that, due to the large breakup probability, in addition to complete fusion (CF) there can be a significant contribution of incomplete fusion (ICF) following breakup of the projectile (e.g., Refs. [7–9]). For the above reasons, a lot of effort has been devoted to the study of fusion reactions around the barrier in collisions induced by halo or, more generally, weakly bound nuclei.

The main experimental challenge of such experiments, especially those using RIBs, at energies below the Coulomb barrier is the low reaction yield due to weak intensity beams and small cross-sections. For this reason thick targets are often used with RIBs in order to increase the yield and reduce the time for measurements. In particular, thick targets, either a single unit or in a stack of them, are often used in activation experiments. These kind of experiments have distinct advantages. As an example, a fusion reaction induced by a beam of light nuclei, such as the halo nuclei presently available at different RIB facilities, on a medium mass target at energies around and below the barrier, will lead to production of low-energy evaporation residues (ER). Direct detection of these slow ERs can be very difficult since, typically, they will be in the same energy range as the β background from the decay of the scattered radioactive beam. Moreover, a large fraction of them may not come out from the target since their energies are too small. However, the activation method takes advantage of this by attempting to capture all the ERs, which

*fisichella@lns.infn.it

come out from the target, by using a stopping foil after it and subsequently deducing fusion cross-sections via on-line or off-line detection of one or more ER radioactive decay channels involving emission of gamma, x-ray, or α radiation. Such an activation method can be made even more efficient if a system of multiple foils, consisting of several target/stopper foils, is used. In this case, the stopper foils also serve to degrade the beam energy for the next target in the stack. The main disadvantage of using a stack is that the beam energy distribution will degrade as the beam traverses the different stack elements due to energy straggling and foils thickness nonuniformities. Therefore, as the beam traverses the stack, it is essential to understand the nature of this degradation in order that accurate excitation functions can be extracted. The need to better understand these degradation effects has been highlighted in recent years by some reported RIB experiments where stacks have been used in order to measure simultaneously reaction yields at a range of beam energies [10–18]. It will be shown in this paper that unless due account is given to the degradation of the beam energy distribution within each target of the stack caused by beam straggling and target nonuniformity, considerable misinterpretation of excitation functions can result, especially at low energies. In previously published papers, generally, not enough information is given concerning the experimental details to assess possible misinterpretations. Therefore the focus of the current paper is to report on a detailed investigation of these degradation effects.

The paper is organized as follows. Section II, following a brief experimental overview, will explore in some detail the traditional methods that have been used to deduce excitation functions from activation data with the stacked target technique, as well as introducing an alternative method based on a deconvolution approach. For this approach a detailed knowledge of the target properties, in particular the target thickness distribution, must be available. This detailed knowledge is contained within the target energy distribution function $D(E,t_0)$ which represents the probability to find a beam particle with energy E inside the considered target of thickness t_0. $D(E,t_0)$ is unique to each target, beam species, and beam energy profile.

Section III addresses the nature and the determination of $D(E,t_0)$. It will be shown that this function can be determined from knowledge of the incoming beam energy distribution, beam ion energy loss, coupled with knowledge of target thickness distribution profile. Section IV will discuss methods to determine target thickness distribution profiles.

Section V will discuss some problems and challenges in the use of thick targets for RIBs experiments by illustrating them through a study of simulations of $^{9}\mathrm{Li} + {}^{120}\mathrm{Sn}$ reaction.

In Sec. VI these different extraction methods to deduce excitation functions will be illustrated by their application to the analysis of new activation data obtained for the fusion reaction $^{6}\mathrm{Li} + {}^{120}\mathrm{Sn}$ experiment performed with nonuniform targets.

Section VII summarizes the conclusions, suggesting the most reliable analysis methods to extract the best estimate of cross-section excitation functions from activation data obtained using the stacked target technique.

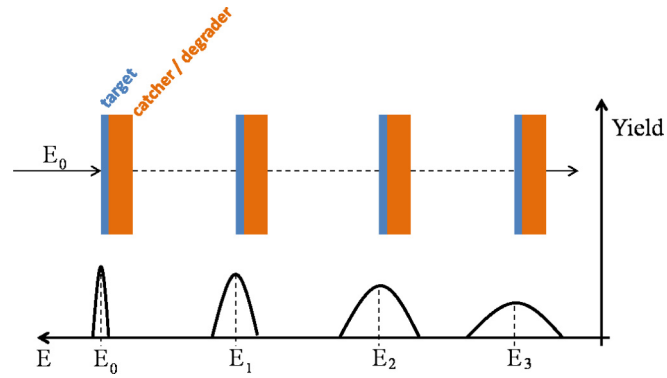

FIG. 1. (Color online) Diagrammatic representation of an activation experiment for measuring the fusion excitation function using the stacked target technique.

II. STACKED TARGET TECHNIQUE

A. Experimental overview

As indicated in Fig. 1, the technique involves using a stack of several target and stopper/degrader foils. The basic idea is that as the beam penetrates the foils, the beam energy will decrease, so the activation produced in different targets will be associated with different mean beam energies.

The stopper foils have two functions: (a) to capture any high energy reaction products escaping from the immediate upstream target and (b) to decrease the mean beam energy for the next downstream target. At the end of the beam irradiation, the activity in each target/stopper foil is monitored over a period of time.

The first foil will be irradiated with average beam energy E_0, and reactions producing activation centers are initiated for beam particles around this energy. The beam then passes through a catcher/degrader foil. However, when the beam enters the second target foil it will have a greater energy spread than for the first target due to the statistical nature of projectile-target interactions and thickness nonuniformity of the first target/catcher foils. This spreading will progressively increase as the beam traverses a greater number of elements in the stack. The activation measured in each target/stopper foil of the stack is therefore the result of an integrated production of ERs over a finite beam energy range. The task of the experimenter is twofold: (1) to accurately measure the ERs activities, and their associated errors, for each target/stopper foil combination and to extract their mean production cross-sections and (2) to relate the measured mean cross-sections to a representative beam energy and thus to the actual cross-section excitation function. The focus of the current paper is on this second task.

B. Relating mean cross-sections extracted with the stack technique to beam energies

The basic experimental data for the stacked target technique are the measured yields, Y, of the ERs. The mean cross-section, σ_{mean}, can be calculated by using the usual relationship:

$$\sigma_{\mathrm{mean}} = \frac{Y}{N_{t_0} N_B}, \tag{1}$$

where N_{t_0} is the number of atoms per unit area of the target and N_B the number of beam particles passing through the target. The problem is how to relate these measured mean cross-sections to effective beam energies in order to accurately match the actual cross-section excitation function, $\sigma(E)$. One way that has been used is to simply relate the measured σ_{mean} to the mean beam energy, defined as:

$$\bar{E} = \frac{E_i + E_f}{2}. \tag{2}$$

Here E_i is the mean energy of the beam particles entering the target and E_f the mean energy of the beam particles after completely traversing the target. E_f is usually determined with the aid of simple energy loss calculations. This approximation is not completely correct, in particular at energies below the Coulomb barrier, since it does not take into account that each reaction energy, inside the target, has a different weight. This is not only due to the energy dependence of the fusion cross-section, $\sigma(E)$, but also due to the beam energy distribution inside the target. In fact, as will be discussed in Sec. III, in general the probability to find a beam particle with a given energy inside the target is a function of the considered energy. For this reason, an alternative proposed definition of effective energy, which at first seems more correct than the previous one, is given by the following weighted average:

$$E_{\text{eff}} = \frac{\int_0^\infty E\sigma(E)D(E,t_0)dE}{\int_0^\infty \sigma(E)D(E,t_0)dE} \tag{3}$$

with

$$D(E,t_0) = \int_0^\infty g(E_0,E_i)\int_0^{t_0} f(E_i,t_0,E,x')dx'dE_i, \tag{4}$$

where $D(E,t_0)$ represents the probability that a beam particle will have energy E inside the considered target of thickness t_0; it will be identified in the following as the *energy distribution function* inside the target. $f(E_i,t_0,E,x')$ is the probability that a projectile incident on the target of thickness t_0 at an incident energy E_i has an energy E at a depth x' inside the target, where $0 < x' < t_0$; $g(E_0,E_i)$ is the probability that a particle, as part of the entrance beam of mean energy E_0, has an energy E_i. In many cases, $g(E_0,E_i)$ is usually considered a Gaussian distribution. It will be shown later that this is not always the case.

Furthermore, other assumptions, which do not seem to be fully justified, in the light of the present results, are sometimes made concerning the averaging procedure to determine E_{eff} (e.g., Ref. [18]). Further discussion of this issue will be reported in Sec. V C.

Moreover, it seems that, in all the previous journal articles the effect of the foil thickness nonuniformity on the beam energy distribution in the stack targets were not considered explicitly. So to explicitly account for target nonuniformity Eq. (4) should include another term, the thickness probability distribution function, $w(t)$, which represents the probability that a particle entering a nonuniform target actually experiences a thickness t. In this case the energy distribution inside the target will be defined as follows:

$$D(E,t_0) = \int_0^{t_0} w(t)\int_0^\infty g(E_0,E_i) \times \int_0^t f(E_i,t,E,x')dx'dE_i dt, \tag{5}$$

with $0 < x' < t$. In this case t_0 represents the maximum target thickness. To determine E_{eff}, by using the Eq. (3) with $D(\text{E},\text{t}_0)$ given by Eq. (4) or Eq. (5), the function $\sigma(E)$ is needed, but this is unknown, and indeed it is the purpose of the experiment. However, a reasonable way to proceed is to relate the measured σ_{mean} to the corresponding $\bar{E}$ of Eq. (2) and use this function to calculate E_{eff}. A new function $\sigma(E_{\text{eff}})$ then can be deduced and used again in Eq. (3) to determine a new E_{eff}. One or two iterations of this nature usually converge to the final value of E_{eff}.

Investigation of Eq. (3), with $D(E,t_0)$ given by Eq. (5), under various conditions leads to interesting insights, since the value of E_{eff} extracted can be equal to, larger than, or smaller than the value of $\bar{E}$ calculated by using Eq. (2). For example:

(1) for a uniform thick target, and for a cross-section independent of beam energy, $E_{\text{eff}} = \bar{E}$;
(2) for a uniform thick target, but where the cross-section increases with increasing beam energy, $E_{\text{eff}} > \bar{E}$, because the higher cross-section weights the yield towards the entrance energy;
(3) for a nonuniform target with a cross-section independent of beam energy, $E_{\text{eff}} < \bar{E}$, since the incoming beam particles can locally explore a target thickness larger than the average one, thus reducing the average interaction energy; and
(4) for a nonuniform target, and when the cross-section increases with increasing beam energy, the effects of (2) and (3) are both relevant. Therefore, E_{eff} can be larger than, smaller than, or equal to $\bar{E}$ depending on the relative weight of the effects (2) and (3).

Clearly, the situation in inferring the actual E_{eff} is quite complex and will depend on the detailed reaction/target parameters for any one case. However, it will shown in the following sections that the procedure to determine $\sigma(E)$ by relating σ_{mean} to E_{eff} is in any case incorrect.

C. Problems with thick targets and large beam energy distributions

As discussed in the previous section, to the present, in all analyses of activation experiments the measured cross-sections, σ_{mean}, have been associated either to the mean energy, $\bar{E}$, or to the effective energy, E_{eff}, based on an energy averaging procedure similar to Eq. (3). In this section, the results of a simple analysis (details given in the Appendix) will show that, in general, neither of these two approaches is correct.

This conclusion already has been implied within experimental studies of nuclear reactions of astrophysical interest, where, due to the very low beam energies combined with the

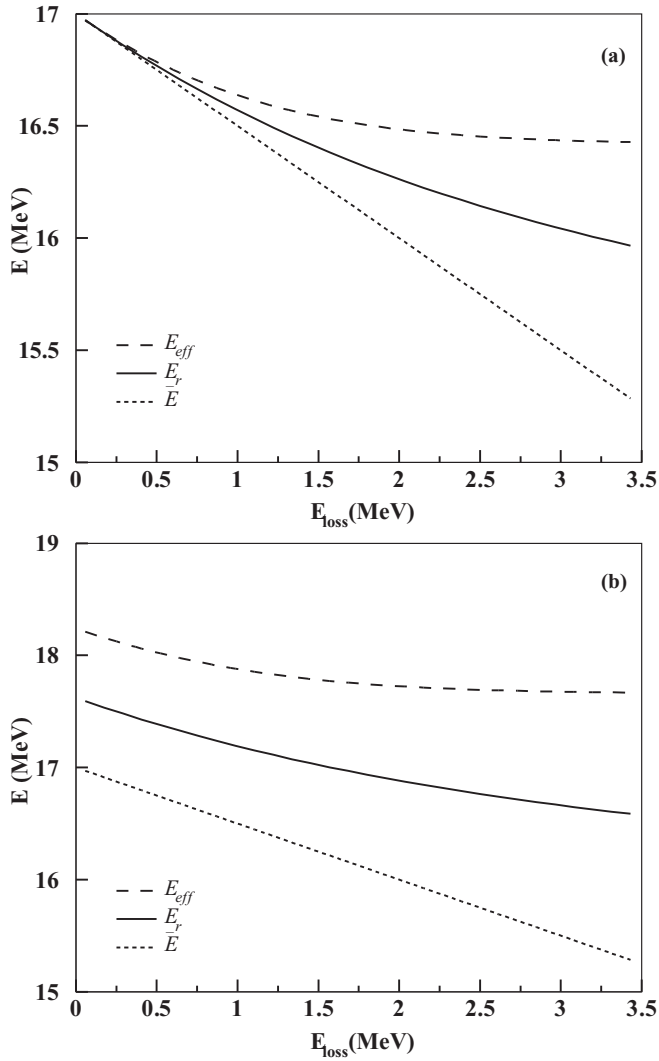

FIG. 2. $\bar{E}$, $E_{\rm eff}$, and E_r for the ^{9}Li + ^{120}Sn reaction, plotted as a function of the energy loss in the target for an average incident beam energy of 17 MeV: (a) δ incoming beam energy distribution and (b) Gaussian incoming beam energy distribution with FWHM = 2 MeV. See text for details.

use of extended gas targets, the effects of the projectile energy loss cannot be neglected [19].

This can be stated in another way. Generally, for the measured cross-section $\sigma_{\rm mean}$, a reaction energy E_r may be defined such that $\sigma_{\rm mean} = E_r$), where $\sigma(E)$ is the true cross-section function. So the data point $(\sigma_{\rm mean}, E_r)$ will coincide with the $\sigma(E)$ curve. Unfortunately, neither the data points $(\sigma_{\rm mean}, \bar{E})$ nor $(\sigma_{\rm mean}, E_{\rm eff})$ will lie on the $\sigma(E)$ curve. In Fig. 2, the values of E_r are compared with the ones of $E_{\rm eff}$ and $\bar{E}$, calculated using the formulas detailed in the Appendix for the ^{9}Li + ^{120}Sn reaction studied in Sec. V. For this calculation it is assumed that the trend of the ^{9}Li + ^{120}Sn sub-barrier fusion excitation function has an exponential trend with a slope $\alpha = 1.72$ MeV^{-1}, obtained from a fit of the exponential part of Eq. (15). Such a slope is with in the range of typical slopes observed in sub-barrier fusion experimental data. The values of the three energies have been calculated for a ^{9}Li entrance energy of 17 MeV and for different energy losses in the target (i.e., targets of different thicknesses). The results shown in Fig. 2(a) correspond to an entrance beam energy of zero energy spread and in Fig. 2(b) to a Gaussian entrance energy spread of 2 MeV FWHM, assuming this spread to be constant within the target. As can be seen, only for the ideal case of a monoenergetic beam and for very thin targets will the three energies coincide. If the beam energy distribution is large, even in the case of very thin targets, $E_{\rm eff}$ and $\bar{E}$ will differ from E_r. The presence of the energy straggling of the beam, and of the target nonuniformities, will further modify this behavior, as noted in Sec. II C, and $\bar{E}$ could even be larger than $E_{\rm eff}$. This demonstrates that one must be very cautious in assigning an energy to measured mean cross-sections, especially in the exponential region of the cross-section, if thick targets and/or large beam energy distributions are used.

D. A deconvolution procedure for analysis of stacked target experiments

Since, in general, neither $\bar{E}$ nor $E_{\rm eff}$ accurately represent the energy E_r to be associated with the measured average $\sigma_{\rm mean}$, the authors have investigated an alternative procedure based on a deconvolution of the stack yields. The outline of this procedure is given below.

The problem of extracting a physically continuous function, like an energy varying cross-section, from a finite number of measurements each of which integrates the function over a wide energy bin is a problem that is encountered in various experimental studies. To be specific, suppose that the physical quantity of interest, z, is a continuous function of the physical parameter, x, such that $z = f(x)$. The experimental objective is to determine this relationship. But the reality maybe that this can only be investigated with an apparatus that integrates z over a range of x in the following manner:

$$z_{{\rm exp},i} = \int f(x) R_i(x) dx, \tag{6}$$

where $z_{{\rm exp},i}$ represents the actual measurement and $R_i(x)$ the response function of the instrument for the particular measurement i. It is assumed that these response functions are well determined. The task is then to extract $f(x)$ from a finite number of such measurements. However, in general, it is not possible to extract a continuous function unambiguously from a finite number of measurements. Nevertheless the level of ambiguity can be considerably reduced if some prior knowledge about the form of the function is available. If this knowledge can be expressed in a *guess function*, $\hat{g}(x,\mu)$, where μ signifies parameters to be determined, then prior predictions can be made concerning $z_{{\rm exp},i}$, i.e.,

$$z_i = \int \hat{g}(x,\mu) R_i(x) dx. \tag{7}$$

The procedure would then be to use this Bayesian prior, and so change μ until $z_{{\rm exp},i}$ and z_i overlap as close as possible when taking account of the errors associated with $z_{{\rm exp},i}$. A recent publication by Jovancevic *et al.* [20] details the above procedure to extract neutron cross-sections from activation data. This is a particularly challenging situation

because such cross-sections vary rapidly with energy, and so special analytical techniques are needed to reduce the ambiguity of deducing $f(x)$ from $\hat{g}(x,\mu)$. If, on the other hand, it is known that $f(x)$ has a smooth varying structure, then a straightforward minimization procedure with respect to μ may be sufficient to quantify $f(x)$. For the experimental situation considered in this paper, the fusion excitation functions $\sigma(E)$ are generally known to be smooth monotonic functions in the energy region near and below the Coulomb barrier. The actual experimental measurements are energy mean cross-sections specified for a particular measurement i by:

$$\sigma_{\text{mean},i} = \frac{\int_0^\infty \sigma(E) D_i(E,t_0) dE}{\int_0^\infty D_i(E,t_0) dE}, \tag{8}$$

where the *response function* $D_i(E,t_0)$ is defined in Sec. II. The task is to deduce the continuous function $\sigma(E)$ from a finite number of values of $\sigma_{\text{mean},i}$. This may be done by quantifying a suitable function $\hat{g}(x,\mu)$ which shows the same expected energy behavior as $\sigma(E)$ and then minimizing the following expression with respect to μ:

$$S = \sum_i \left(\frac{\sigma_{\text{mean},i} - \hat{g}_{\text{mean},i}}{\beta_i} \right)^2, \tag{9}$$

where

$$\hat{g}_{\text{mean},i} = \frac{\int_0^\infty \hat{g}(E,\mu) D_i(E,t_0) dE}{\int_0^\infty D_i(E,t_0) dE} \tag{10}$$

and β_i is the experimental error associated with $\sigma_{\text{mean},i}$.

Application of the procedures described in this section requires detailed knowledge of $D(E,t_0)$. As will be described in the next section, $D(E,t_0)$ can be deduced with reasonable reliability with modern codes such as SRIM [21,22]. If the targets are nonuniform, then it is necessary to know the target thickness probability distribution, $w(t)$, for determining $D(E,t_0)$; the method, developed by the present authors, to determine $w(t)$ will be outlined in Sec. IV.

III. DETERMINATION OF THE ENERGY DISTRIBUTION FUNCTION $D(E,t)$ FOR UNIFORM FOILS

As explained in Sec. II B, the energy distribution inside the target, $D(E,t_0)$, represents the probability to have a beam particle with energy E inside the considered target of thickness t_0. According to Eq. (5), to determine $D(E,t_0)$ it is necessary to know the particle energy probability distribution before the target, $g(E_0,E_i)$, and $f(E_i,t,E,x)$, i.e., the probability that an incoming ion of energy E_i will have energy E at a generic depth x inside the target. The SRIM code has been used for determining $f(E_i,t,E,x)$ and $g(E_0,E_i)$. The $f(E_i,t,E,x)$ function has been determined by the following procedure. For each incoming energy E_i of the beam particles a full SRIM simulation has been performed considering gradually increasing target layers, ranging from 0 mg/cm^2 to the maximum value of the target thickness. The probability distribution $f(E_i,t,E,x)$ is the energy distribution after a thickness x. For each incoming energy E_i the $f(E_i,t,E,x)$ distributions obtained for each layer x have been summed over x. In order to obtain the final $D(E,t_0)$ distribution, for all incoming energies given by the $g(E_0,E_i)$ distribution, a weighted sum over E_i has been performed. This procedure is formally expressed by Eq. (4). Since the $f(E_i,t,E,x)$ is determined from multiples histories of many particles, straggling effects are accounts for.

These simulations showed that the determination of the beam energy distribution in a target is not trivial when using a stack, since it depends not only on the features of the single target but also on the targets placed upstream. Moreover, this kind of study was particularly useful since it illuminates many of the subtle effects of the stacked target technique. These effects, which influence the extraction of accurate cross-sections, are even significant if the target foils used are thinner than those often used in RIB experiments. As examples of such simulations (which will be relevant to the experimental situations discussed in Secs. V and VI), the $D(E,t_0)$ distributions have been calculated for the following two situations: (a) a ^{120}Sn uniform target 0.5 mg/cm^2 thick directly irradiated by a ^{6}Li beam of 18.44 MeV and (b) a target which is the fourth in a stack of uniform Sn foils (0.5 mg/cm^2 thick) and uniform ^{93}Nb (2 mg/cm^2 thick) catchers but with an increased ^{6}Li energy entering the first target in the stack so the average energy entering the fourth target is the same energy as the almost monoenergetic beam used for (a). The two corresponding $D(E,t_0)$ distributions are shown in Fig. 3.

The $g(E_0,E_i)$ distribution, in the case of the single foil irradiation, depends only on the characteristics of the beam delivered by the accelerator. In the example of Fig. 3, it has been assumed that $g(E_0,E_i)$ for situation (a) has a Gaussian shape with a full width at half maximum (FWHM) of 0.1%. For a target placed in a stack, $g(E_0,E_i)$ will again depend on the characteristics of the beam delivered by the accelerator but is generally dominated by the energy straggling in the foils placed upstream. To take this into account, $g(E_0,E_i)$ for situation (b) has to be calculated (using SRIM) by considering all the foils upstream. For the two cases the energy distribution function inside the target has a different shape. It is found that the rectangular shape obtained in the case of the single foil measurement is typical of targets irradiated by a beam whose input energy distribution FWHM is smaller than the average energy loss, ΔE, in traversing the target. However, when the FWHM of the beam energy distribution before a target is larger than ΔE (caused by energy straggling of upstream foils in a stack), the shape will be Gaussian like. In addition, the energy range of the energy distribution inside the target will differ from when a single foil alone is used. This means that, even if the average incoming energy and the target thickness are the same, the measured cross-section is integrated over different energy regions in the two cases. This difference is due to the different widths of the two incoming energy distributions. The region inside the red lines in Fig. 3 represents the energy range estimated by performing an energy loss calculation, without taking into account the finite width of the energy distribution. This is a good approximation in the case of single foil irradiation, but it is half of the energy range observed in the stack case. In view of this observation, the integration range cannot be determined by simply performing an energy loss calculation, since it would lead to an underestimation of the real beam energy range inside the target. Of course, this effect becomes more and more important as the number of targets

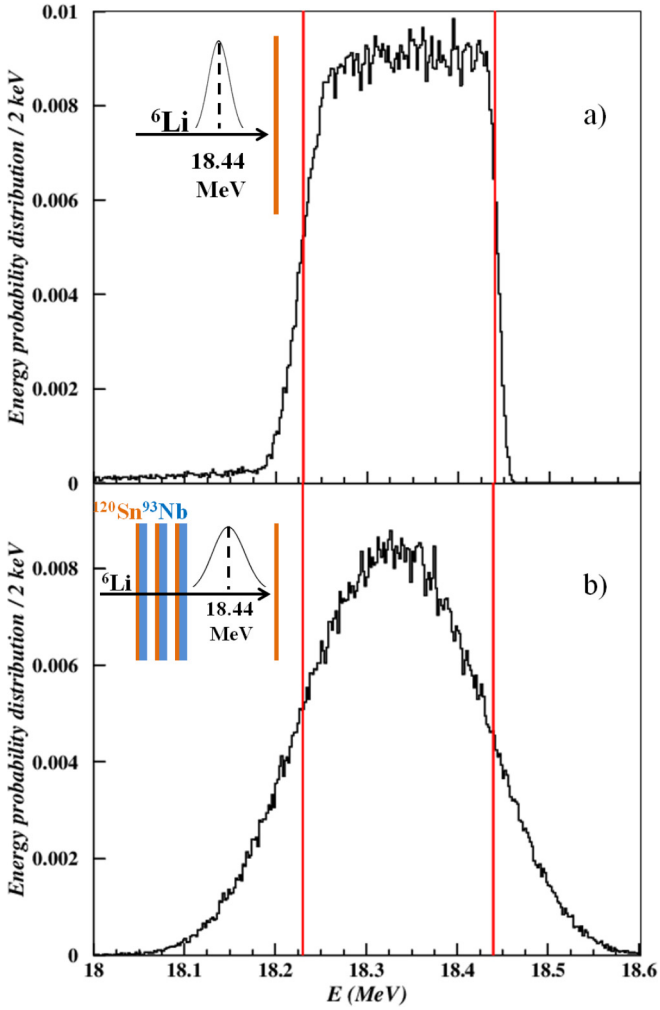

FIG. 3. (Color online) Beam energy distribution function $D(E,t_0)$ seen by a Sn target 0.5 mg/cm^2 thick, for an average incoming energy of 18.44 MeV in two different conditions: (a) Sn target directly irradiated by the beam (b) Sn target placed in a stack after three Sn foils (0.5 mg/cm^2 thick) and corresponding ^{93}Nb (2 mg/cm^{2}thick) catcher foils. See text for details.

in the stack increases. It is important to emphasize that the energy spread in the distribution shown in Fig. 3 is only due to the statistical nature of the energy loss process. A further contribution to the broadening of the energy distribution can arise from the nonuniformity of the foil thickness, which will cause an additional spread of the energy distribution inside the target. A systematic account of such nonuniformities and their effect on the energy distribution in target stack systems seems not to have been explicitly reported previously in the literature. However, for energy regions where the fusion cross-section decreases rapidly with decreasing energy, the target ER yields are very sensitive to precise width and shape of the beam profile. Therefore in the present work an investigation has been undertaken to analyze the effects of target nonuniformity and how this affects the determination of the energy distribution function $D(E,t_0)$.

IV. CHARACTERIZATION OF FOILS

A. Surface morphology

The most important issue for the stacked target technique is the production of quality targets and degrader foils; quality here refers to uniformity of thickness and stoichiometry. Production of such quality foils is in the province of surface science, which has greatly expanded in recent years. The laying down of a thin layer of one type of material on another can be obtained by a variety of techniques such as a chemical deposition, evaporation, or sputtering. In any one method the condition to achieve a uniform deposit can be quite complex. For example, the structure of thin films is affected by different factors, namely by the type of the substrate, the thickness of the film, the deposition rate, and the temperature of the substrate [23–27]. For the stacked target technique the optimum situation is to produce foils of the best mass density uniformity. However, for a particular production technique and target material, which could also be an expensive rare isotope available in limited quantities, obtaining such high uniformity may not be possible in all cases. Nevertheless, it will be shown in this paper that, provided certain procedures are followed, it is possible to use the stacked target technique even if the targets are considerably nonuniform, providing certain precautions are followed.

The procedure, developed by the present authors, for the characterization of foil nonuniformity will be highlighted in the following. In particular, analyses performed on composite ^{120}Sn - ^{93}Nb foils, produced by the evaporating ^{120}Sn-enriched isotope on rolled ^{93}Nb foil substrate, will be reported. These foils were used for measuring the ^{6}Li + ^{120}Sn fusion excitation function $\sigma_{\rm fus}(E)$ by the stack technique, reported in Sec. VI. The targets were manufactured at Laboratori Nazionali del SudINFN, Catania. The average thickness of these foils was determined by weighting the foils and by measuring the energy loss of α particles from an ^{241}Am source traversing the foils.

For investigating the surface morphology of the targets, a scanning electron microscope (SEM) Zeiss Supra 25 was used. The SEM analysis was performed at the Institute of Microelectronics and Microsystems (CNR-IMM), Catania. The results are shown in Fig. 4(a) for a ^{93}Nb backing foil and in Fig. 4(b) for a composite ^{120}Sn - ^{93}Nb foil. The ^{93}Nb foil has an average thickness of 2 mg/cm^2, and its surface does not show any particular features on the scale of μm. This observed surface morphology is typical of rolled foils where small defects seem randomly distributed on the foil surface. The ^{120}Sn layer has an average thickness of 0.5 mg/cm^2 (about 0.7 μm). On its surface it is possible to distinguish structures of different sizes, which vary from some hundreds of nm to about 2 μm. The same kind of analysis was also undertaken on some foils where the ^{120}Sn was evaporated onto a rolled ^{165}Ho substrate. As for the ^{93}Nb foil, the ^{165}Ho foil does not have particular structures. The ^{120}Sn surface for this case shows the same kind of structures as observed in Fig. 4(b). It is therefore concluded that the surface ^{120}Sn structures are intrinsic to the properties of ^{120}Sn rather than the properties of the backing foil. These ^{120}Sn target foils are clearly not uniform in thickness and therefore present

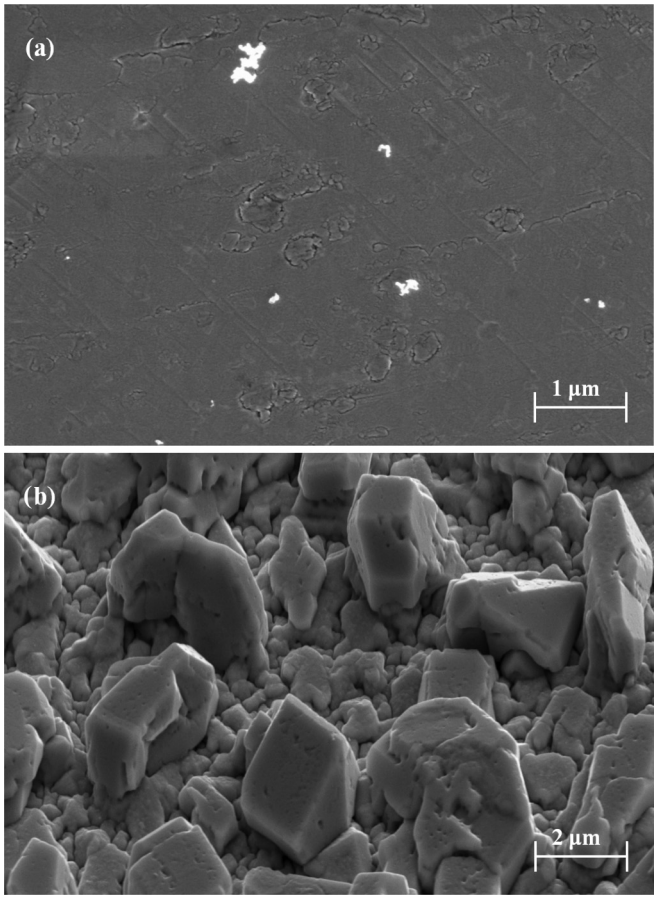

FIG. 4. Scanning electon microscope views of the surfaces of a ^{120}Sn target evaporated onto a rolled ^{93}Nb foil: (a) ^{93}Nb side and (b) ^{120}Sn side. See text for details.

a considerable challenge to deduce $D(E,t_0)$ for a particular reaction of interest. It will be shown below that this challenge can be met if certain procedures are followed.

B. Determination of the thickness probability distribution $w(t)$

To investigate quantitatively the nature of foil nonuniformity, a procedure based on the analysis of the energy spectra of transmitted ^{241}Am α particles has been used. The residual energy spectra of the α particles traversing the ^{93}Nb substrate and the ^{120}Sn + ^{93}Nb foil are shown in Figs. 5(a) and 5(b) (dashed black line); the figures also show the corresponding spectra obtained from SRIM simulations (continuous red line) assuming a uniform target of the same measured average thickness. For the sake of comparison, the spectra have been normalized so the figure areas below the two histograms are the same. As can be seen, the simulation spectra do not reproduce the experimental data, but while in the case of the ^{93}Nb foil the measured and simulated curves have a Gaussian shape, although with different widths, in the case of ^{120}Sn + ^{93}Nb foil, the shape of the experimental distribution is not Gaussian anymore. The ^{120}Sn thickness (in mg/cm^2 and in μm) which α particles must pass through in order to produce the measured residual energy is shown on the lower axes. It can be seen that (i) the zero thickness of the ^{120}Sn corresponds to the average

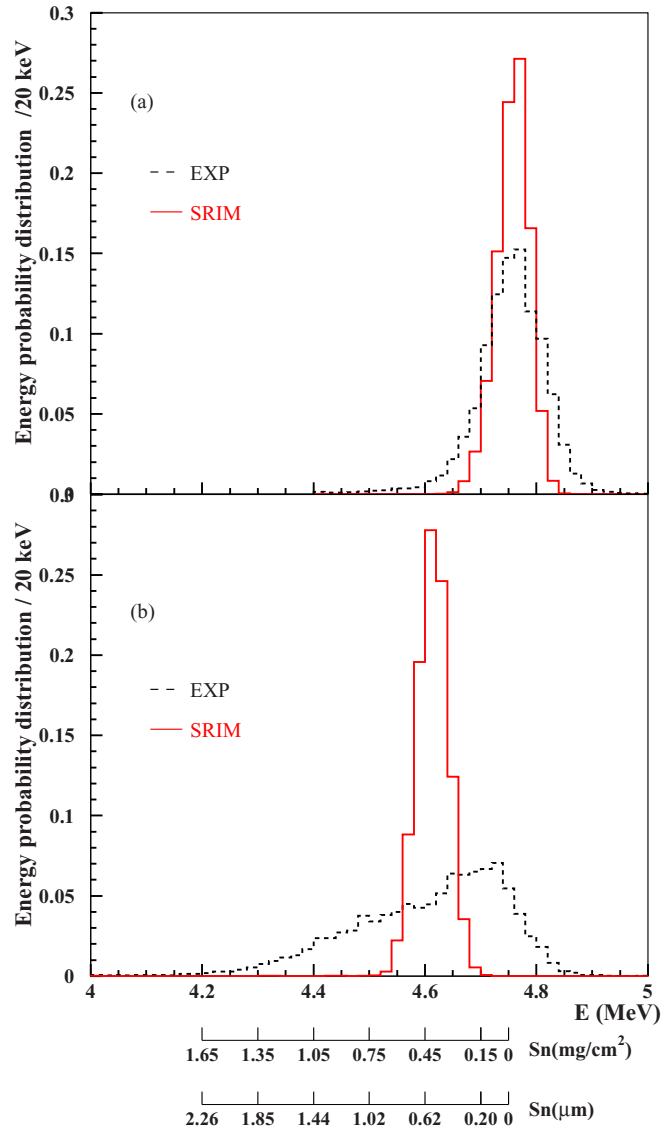

FIG. 5. (Color online) Experimental (black dashed line) and simulated (red line) energy spectra of α particles emitted by an ^{241}Am source passing through a ^{93}Nb foil (a) and through a ^{120}Sn + ^{93}Nb foil (b). The simulated spectra are obtained by using the SRIM [22] code. The lower axes indicates the ^{120}Sn thickness which the α particles have to pass through to produce the observed residual energy.

thickness of the substrate and (ii) the ^{120}Sn thickness reaches the values 1.5 mg/cm^2 (2 μm), which is compatible with that expected from surface features observed with the SEM scans shown in Fig. 4(b).

For determining the ^{120}Sn thickness probability distribution the following procedure was followed. By using the SRIM code, residual energy spectra for α particles emitted by an ^{241}Am source, which traverse a ^{120}Sn + ^{93}Nb foil, were determined for various ^{120}Sn thicknesses ranging from 0 mg/cm^2 to 1.5 mg/cm^2. A weight was attributed to each individual spectrum such that their weighted sum could reproduce the experimental spectrum. Let n be the number of spectra and W_j (with $j = 1,n$) the set of the attributed weights. The W_j

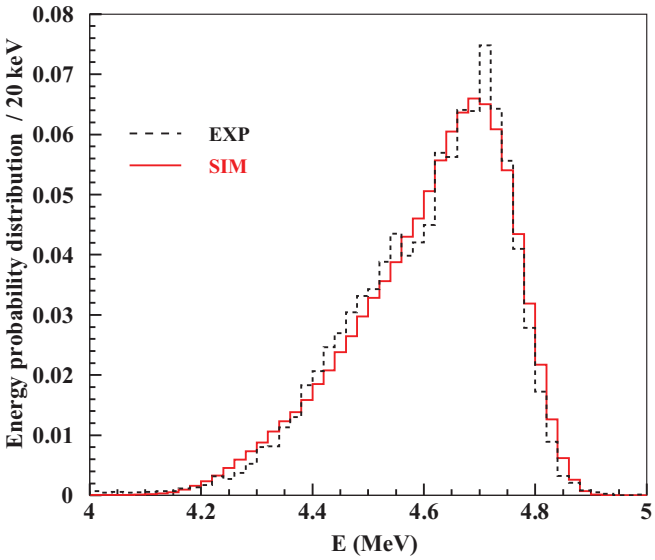

FIG. 6. (Color online) Experimental (black dashed line) residual energy spectrum of α particles crossing a ^{120}Sn + ^{93}Nb foil. The red spectrum is the result of the fit procedure used to extract the ^{120}Sn thickness probability distribution (see text for details).

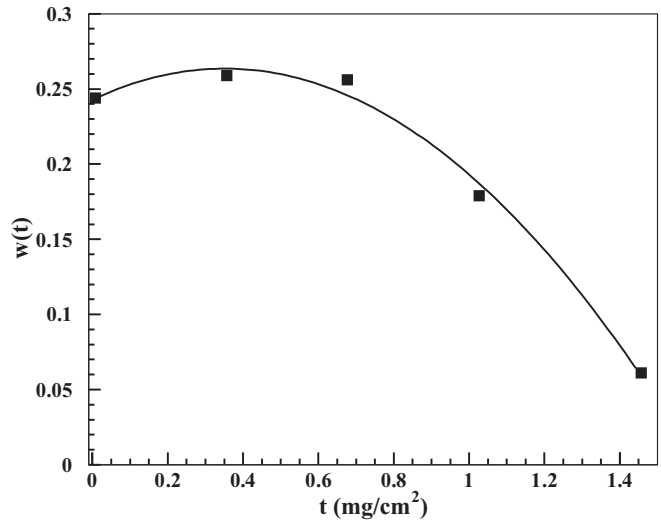

FIG. 7. ^{120}Sn target thickness distribution.

were varied, from 0 to 1 in steps of 0.01, in order to obtain the best match between the simulated and the experimental spectra. In particular, the chosen weights were the ones which minimized the χ^2 defined as follows:

$$\chi^2 = \left[\sum_{i=1}^{m} \frac{(C_{\mathrm{sum},i} - C_{\mathrm{exp},i})^2}{C_{\mathrm{exp},i}}\right] \Big/ m, \qquad (11)$$

where m is number of bins of the spectra and $C_{\mathrm{exp},i}$ and $C_{\mathrm{sum},i}$ are the number of the counts in the generic bin i in the experimental and the summed simulated spectrum, respectively. In particular, $C_{\mathrm{sum},i}$ has been obtained as $\sum_j C_{ji} W_j$, where C_{ji} are the counts in bin i of the j spectrum. The weights W_j, obtained as described above, after normalization give the target thickness probability distribution $w(t)$. In Fig. 6 the experimental residual energy spectrum of α particles crossing a single ^{120}Sn + ^{93}Nb foil is shown together with the simulated one obtained as the result of the minimization procedure. In Fig. 7 the relative $w(t)$ trend for the ^{120}Sn target is reported as function of the thickness. The continuous line is a polynomial fit of the the calculated weight E_r. The number of simulated spectra was chosen as the minimum necessary to obtain a flat distribution, when each one was given a weight equal to one.[1] In the present case, the explored range of interest has been covered by using five simulated spectra. Such a procedure is general and can be applied to foils of any thickness distribution. However, when the residual energy spectra of α particles crossing the foil have a quasi-Gaussian symmetric shape, as for ^{93}Nb foils showed in Fig. 4(a), a simplified procedure can also be applied. In such cases, the contribution to the FWHM due to the foil nonuniformity can be determined by using the following relationship:

$$\mathrm{FWHM}^2_{\mathrm{exp}} = \mathrm{FWHM}^2_{\mathrm{coll}} + \mathrm{FWHM}^2_{\mathrm{res}} + \mathrm{FWHM}^2_{\mathrm{nonunif}}, \qquad (12)$$

where $\mathrm{FWHM}_{\mathrm{exp}}$ is the full width at half maximum of the experimental transmitted α energy spectra and $\mathrm{FWHM}_{\mathrm{coll}}$, $\mathrm{FWHM}_{\mathrm{res}}$, and $\mathrm{FWHM}_{\mathrm{nonunif}}$ are, respectively, the FWHM due to the statistical nature of the energy loss process, the intrinsic detection resolution (which is about 40 keV), and the foil thickness nonuniformity. From Eq. (12) it is possible to determine the $\mathrm{FWHM}_{\mathrm{nonunif}}$ and thus to estimate the thickness variation, Δt, needed to explain such a straggling by using the relationship:

$$\Delta t = \frac{\mathrm{FWHM}_{\mathrm{nonunif}}}{(dE/dt)_{\mathrm{AV}}}, \qquad (13)$$

where $(dE/dt)_{\mathrm{AV}}$ is the average rate of beam energy loss in the target of thickness t. With this procedure it has been estimated that the nonuniformities in thickness for ^{93}Nb foils are of the order of 7% of the average value.

C. Validation of the procedure for determining $w(t)$

In order to check the procedure developed for determining the ^{120}Sn thickness probability distribution, measurements were made of the residual energy spectrum of a 21-MeV ^{6}Li beam after traversing one and then three target foils. These measurements were undertaken by placing a detector behind each target combination. The foils and the detector were placed at 20° with respect to a thin (0.1 mg/cm^2) Au target. A 3-mm collimator was placed in front of the foils in order to reduce the kinematic broadening of the scattered beam.

The experimental residual energy spectra for the one and three target foil measurements are shown with the black continuous line in Figs. 8(a) and 8(b), respectively. As is possible to see, the beam energy distribution after traversing the first foil of the stack is not Gaussian. The shape of this distribution is dominated by the target nonuniformity, as it

[1]For the sake of clarity, it may be useful to remark that if a target is uniform, then $w(t)$ would be a δ function; if the target has a small random thickness variation, then $w(t)$ would more likely be a Gaussian-type function centered at the average thickness.

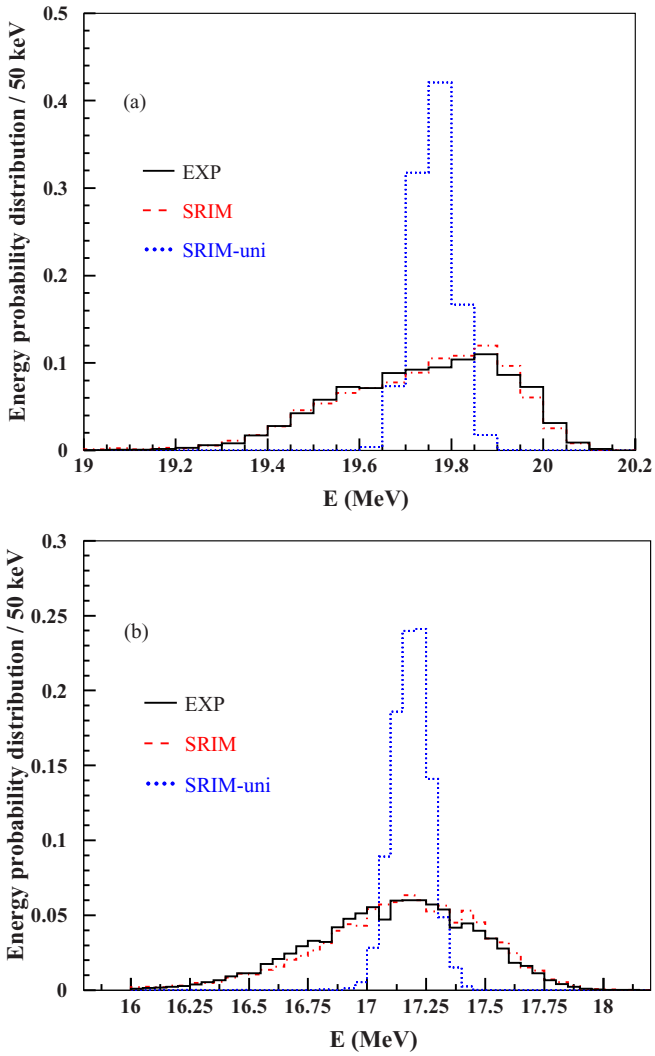

FIG. 8. (Color online) Experimental (black continuous line) and simulated (red dashed line) residual energy spectra of a 21-MeV ^{6}Li beam, after traversing one (a) or three (b) ^{120}Sn + ^{93}Nb foils. The blue dotted lines give the calculated residual energy distributions for the case where the ^{120}Sn and ^{93}Nb foils are uniformly thick with the same total thickness as the nonuniform foils. See text for details.

was previously observed for the α-spectra measurements. Concerning the beam distribution after the third foil of the stack, its shape is more similar to a Gaussian distribution, but its width is 3 times wider than the one expected if the foils were uniform. Presumably, the Gaussian shape for the three-foil combination is the result of increased randomization of different thicknesses encountered by the beam as compared to the transit of just one foil.

By using for each target and catcher the previously determined $w(t)$, (as discussed above by the α-particle ranging technique), SRIM simulations were performed to determine the expected energy spectra for the 21-MeV ^{6}Li beam after traversing one and three foils; these simulated spectra are shown as red dashed lines in Figs. 8(a) and 8(b). As one can clearly see from this figure, the experimental ^{6}Li energy distribution is very well reproduced by the simulation. It must be stressed that this agreement is only possible because each foil was characterized by its own unique $w(t)$ distribution. The blue dotted lines give the calculated residual energy distributions for the case where the ^{120}Sn and ^{93}Nb foils are uniformly thick with the same total thickness as the nonuniform foils. This comparison is interesting since it gives a "direct view" of the importance of such nonuniformity effects.

It is particularly interesting to note that the use of the target thickness probability distribution, $w(t)$, obtained by using an α-particle source as discussed in Sec. IV B, was of sufficient accuracy as to allow reasonable reproduction of the energy distribution observed with the actual ^{6}Li beam. This is an important point because, as will be shown in the following, for the correct determination of the fusion excitation function, the actual individual target thickness distributions, and not just the average thicknesses, must be determined for all targets. However, this work demonstrates that the thickness probability distribution $w(t)$ can be extracted simply by using an α-particle source rather than requiring additional beam time. The good matching between the experimental spectra for the three-foil system [Fig. 8(b)] gives us confidence that the procedure to determine the different target $w(t)$ functions is valid, and the procedure used is accurate enough to determine the $D(E,t_0)$ functions.

V. PROBLEMS AND CHALLENGES RELATED TO THE USE OF THE STACKED TARGET FOR RIBS EXPERIMENTS

A. Introduction

For the reason mentioned in the Introduction, the stacked target technique as been widely used in experiments with RIBs. Many experiments have been performed where the beam is passed through a large number of stacked targets and degrader foils (e.g., $\sim$ 30 foils in Ref. [11] and up to 24 foils in Ref. [16]). Moreover, in some cases, in order to compensate for the low RIB currents, quite thick foils (e.g., 26 mg/cm^2 Au targets [16] and 10 mg/cm^2 Al degraders [17]) have been used, with corresponding large energy variations between the first and last target of the stack (e.g., $\sim$10 MeV in Refs. [11,15] and up to $\sim$40 MeV in Ref. [16]).

Due to the large number of foils, and/or their nonuniformities, and/or the quality of RIBs used, in many experiments, targets have been irradiated by beams having rather large energy dispersion (e.g., up to $\sim$6 MeV FWHM in Ref. [15], 1.6 MeV FWHM on the first of 16 foils in Ref. [11], $\sim$2 MeV FWHM on the first of three targets in Ref. [12], and up to 56 MeV FWHM in Ref. [16]). Generally, in the journal articles for these multiple/thick target experiments, very limited quantitative information is given of target nonuniformity, straggling effects, and incident beam quality. However, these factors can significantly influence the deduced excitation functions due to the potentially large beam energy distribution inside the targets. In order to quantify the magnitudes of these effects, the results of simulations concerning a possible future ^{9}Li + ^{120}Sn experiment are discussed in Sec. V B.

The Sec. V C will discuss how these effects could impact in the interpretation of the previously published data.

B. Simulation study of the ^{9}Li + ^{120}Sn fusion reaction

For this study a simulation was undertaken by investigating the outcome when a ^{9}Li beam of about 28.1 MeV impinged on a stack of five targets each composed of ^{120}Sn foils with an average thickness of 5 mg/cm^2, each one followed by an uniform ^{93}Nb catcher/degrader foil 1.5 mg/cm^2 thick. The results of the simulations were studied for the case of uniform targets and degrader foils and for the situation where both targets and foils are nonuniform. Two different kinds of nonuniformities were investigated; one where a Gaussian thickness distribution with a FWHM of 20% of the mean value was considered for the ^{120}Sn targets, and a second one where the ^{120}Sn targets where assumed to have a nonuniformity similar to the ones actually observed experimentally and reported in Sec. IV (i.e., the surface of the targets is characterized by the presence of structures which vary from few hundred nm to 2 μm, like the ones shown in Fig. 4). In the following, this second kind of nonuniformity will be called polynomial nonuniformity. For both uniform and nonuniform targets the average thickness is assumed to be 5 mg/cm^2. The ^{93}Nb catcher foils were assumed to have a Gaussian nonuniformity with a FWHM of 15% of the mean value. For each target, the mean cross-section that would be measured in the considered experimental conditions, due to the energy distribution inside the target, has been calculated by the following relation:

$$\sigma_{\text{mean}} = \frac{\int_0^\infty \sigma(E) D(E,t_0) dE}{\int_0^\infty D(E,t_0) dE}. \quad (14)$$

The $D(E,t_0)$ distributions, for each of the considered cases, were calculated by using the program SRIM, and it was assumed that the real fusion cross-section $\sigma(E)$ is given by a Wong-like formula [28]:

$$\sigma(E) = \frac{A}{E} \ln[1 + e^{B(E-C)}] \quad (15)$$

with $A = 1936$ mb MeV, $B = 1.83\,\text{MeV}^{-1}$, and $C = 18.95$ MeV. It is important to note that the difficulty of relating the measured values of σ_{mean} to the actual $\sigma(E)$ function, becomes more severe as the slope of $\sigma(E)$ becomes steeper. The chosen parameters in Eq. (15) are consistent with the cross-section slopes of other similar reactions. Figures 9(a) and 9(b) show the entrance and exit beam energy distributions, respectively, for the first target of the stack. Figure 9(c) shows the corresponding $D(E,t_0)$ functions. The black continuous, the red dashed, and the blue dotted lines correspond to the case of uniform, nonuniform Gaussian, and non-uniform polynomial target thickness distributions. Figure 10 is the same as Fig. 9 but for the fifth target of the stack. It can be seen that, as expected, the outgoing energy distribution for a given target is wider for the nonuniform cases when compared to the uniform one, while the average value is the same. Similarly, the energy distributions $D(E,t_0)$ [Figs. 9(c) and 10(c)], even if the average target thickness is the same in the three cases, are wider for the nonuniform targets.

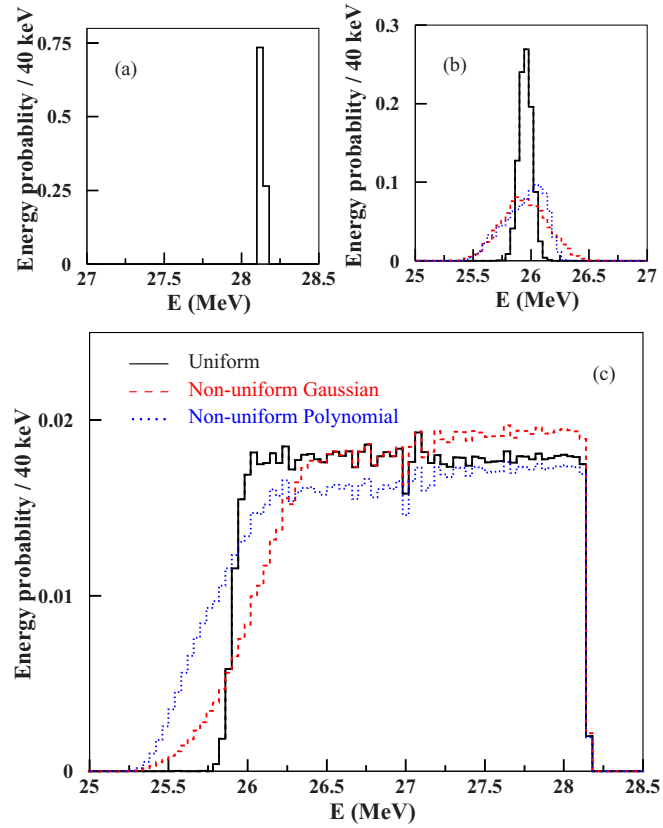

FIG. 9. (Color online) Energy distribution of the beam before (a), after (b), and inside (c) the first target of the stack considering uniform (black continuous line), nonuniform Gaussian (red dashed line), and nonuniform polynomial (blue dotted line) foils. See text for details.

At this point it is important to emphasize the physical factors that influence the shape of the energy distribution function $D(E,t_0)$. These factors include the shape of the beam energy distribution entering the target, the beam energy loss in the target, and the energy straggling of the beam. Inspection of Figs. 9(c) and 10(c) shows that, as a result of these factors, $D(E,t_0)$ cannot be approximated by assuming it to be a shape similar to the entrance distribution (i.e., Gaussian), having an energy width intermediate between the width of the entrance and the exit energy distributions. It must be stressed that the best way to determine $D(E,t_0)$ is to characterize target properties, as well as to perform numerical beam energy loss simulations. In this way it should be possible to quantify all of the physical factors that influence the shape of $D(E,t_0)$ shown in Figs. 9(c) and 10(c).

In Fig. 11 the σ_{mean} given by Eq. (14), which would be measured using the considered stack of targets, for the uniform [Fig. 11(a)] and nonuniform target [Fig. 11(b)] cases, is plotted versus the mean energy $\bar{E}$ (closed symbols) and versus the effective energy E_{eff}(open symbols). It should be borne in mind that the yield values that would be measured for the three cases differ due to the different energy distributions inside the targets. The E_{eff} has been obtained by using Eq. (3) and

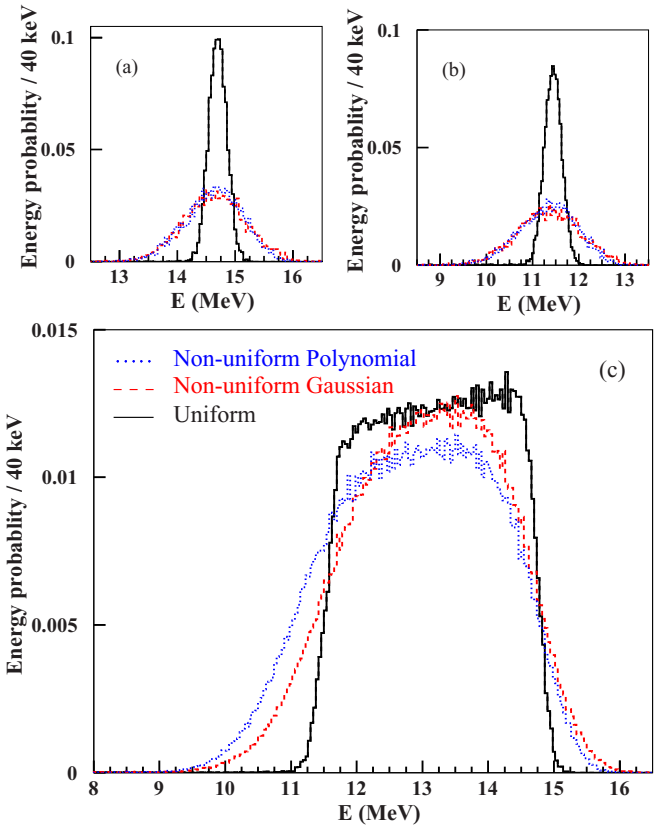

FIG. 10. (Color online) Energy distribution of the beam before (a), after (b), and inside (c) the fifth target of the stack considering uniform (black continuous line), nonuniform Gaussian (red dashed line), and nonuniform polynomial (blue dotted line) foils. See text for details.

$D(E,t_0)$ given by Eq. (4) and Eq. (5) in the case of uniform and nonuniform target thickness, respectively. In Fig. 11(b) the up-triangles are the results obtained in the case of Polynomial nonuniformity of the target, and the squares are the results obtained for the Gaussian nonuniformity. The continuous line represents the cross-section of Eq. (15) assumed to represent the real behavior of the fusion excitation function in the simulated experiment. As one can see in Fig. 11, at energies below the Coulomb barrier, the real excitation function is not reproduced by any of the various representations. Associating $\sigma_{\rm mean}$ to $\bar{E}$ or to $E_{\rm eff}$ produces an overestimation or an underestimation of the real excitation function, respectively, in agreement with the simple estimation shown in Fig. 2. The tables in the insets of the Fig. 11 report the ratios between $\sigma_{\rm mean}$ that would be measured, in the fourth and fifth targets of the stack, and the values of the starting cross-section $\sigma(E)$ calculated at $\bar{E}$ and $E_{\rm eff}$. These ratios are larger in the case of nonuniform targets than for uniform ones due to the wider energy distributions $D(E,t_0)$, as shown in Figs. 9(c) and 10(c). As can be seen, in the present case, plotting the measured cross-sections versus $\bar{E}$ or $E_{\rm eff}$ generates differences up to a factor of 5 with respect to the real fusion excitation function $\sigma(E)$.

The deconvolution procedure discussed in Sec. II D has also been applied to the present simulated data. For this procedure

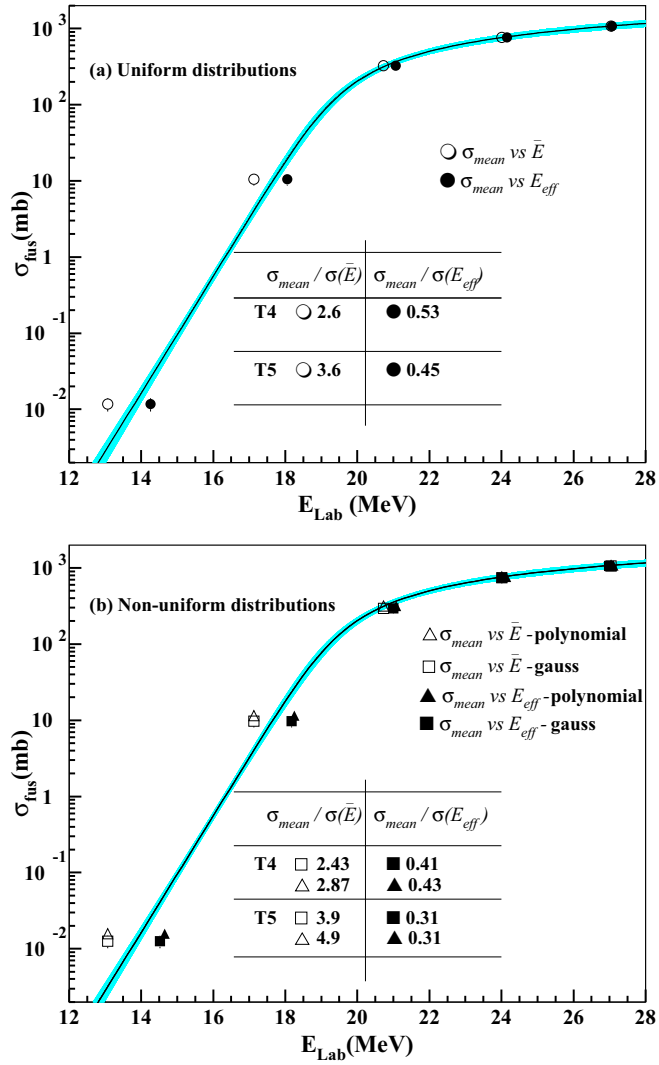

FIG. 11. (Color online) Results of the simulations for the cases of uniform (a) and nonuniform (b) targets. The continuous black line shows the *real* fusion excitation function assumed for the collision ^{9}Li + ^{120}Sn. The open and closed symbols are the experimental results that would be obtained plotting the measured $\sigma_{\rm mean}$ versus $\bar{E}$ and $E_{\rm eff}$. In (b) the triangles and square symbols are the results of the simulation performed considering two different kind of nonuniformities: Gaussian and polynomial. In this figure the results of the deconvolution procedure, discussed in Sec. II D, cannot be distinguished from the black line. The blue shaded area represents the uncertainty associated with the deconvolution procedure. (See the text for details.)

a typical error on the measured mean cross-section, $\sigma_{\rm mean}$, in each of the targets has been supposed to be 15% of the mean value. This error would originate from experimental uncertainties associated with detector efficiencies, mean target thickness, target thickness distribution, etc. As shown in Fig. 11, the results obtained with this procedure cannot be distinguished from the continuum line representing the assumed real cross-section. The shaded area represents the error band associated with the deconvolution procedure. This error band has been calculated by applying the standard error propagation formula (see, e.g., Ref. [29]) to Eq. (15),

considering the three parameters (A, B, and C) as free variables. This procedure takes account of the error on the single variables as well as possible correlations between the variables of the function through the covariance terms of the error matrix. This deconvolution procedure has been performed by using the MINUIT routine [30], which also provides the error parameters and the covariance terms.

Since, in this case, σ_{mean} is not a measured value but the result of a numerical procedure, the meaningfulness of the error band has been cross checked in the following way. By using a Monte Carlo simulation, several sets of five possible values of cross-sections, s_i (one for each target), were determined, extracting each s_i value from a Gaussian distribution, centered at the calculated $\sigma_{\text{mean},i}$ value and having a standard deviation equal to $0.15\sigma_{\text{mean},i}$. For each extracted data set, the deconvolution procedure was applied. The resulting deconvoluted curves all lie within the shaded area of Fig. 11, indicating consistency between the two approaches.

In conclusion, plotting the mean cross-section, which represents what would be measured in a real experiment, as a function of $\bar{E}$ or E_{eff} is not representative of the real excitation fusion function, due to the finite beam energy distribution inside the targets. The opinion of the present authors is that the best method for determining the fusion excitation function is the application of a deconvolution procedure. Having determined the excitation function, therefore, it would be possible to determine the E_r as outlined in the Appendix. However, since the excitation function has been determined, calculation of the E_r is somewhat superfluous.

The present authors also underline that these kinds of problems could also be present if thin targets are used. In fact, as already mentioned, it is not the target thickness itself but rather the width of the energy distribution inside the target $D(E,t_0)$ which is the origin of the problem. In fact, under certain circumstances, large energy widths for $D(E,t_0)$ can be present even with thin targets, e.g., if one has several foils, and/or thick nonuniform catchers, and/or poor quality RIBs.

To make this clearer, simulations were undertaken for a very thin uniform ^{120}Sn target irradiated with ^{9}Li beams at fixed average incoming energy of 17 MeV (see inset of Fig. 12) but for different FWHM of the incoming Gaussian beam energy distribution in the range 0.3 to 4 MeV. This range is chosen because, as mentioned in Sec. V A, experiments have been performed with energy beam dispersions in the range 26 MeV FWHM. The average energy loss, in traversing the target, is of about some hundreds keV. So, even if the target thickness and the centroid of the incoming beam energy distributions are always the same, the value of the cross-section σ_{mean} obtained by Eq. (14), that would be measured for the considered target, will be different for each one of the considered incoming distributions, due to the different explored beam energy range. In Fig. 12, the continuous line is the cross-section of Eq. (15) assumed to represent the real behavior of the fusion excitation function; the circles and the triangles represent the simulated value of "measured" cross-section, σ_{mean} plotted either versus E_{eff}, calculated by Eq. (3), with $D(E,t_0)$ given by Eq. (5), or $\bar{E}$ calculated by Eq. (2), respectively. The σ_{mean} and the E_{eff} all depend on the FWHM of the incoming 17-MeV beam. A good agreement between the "real" function and the data

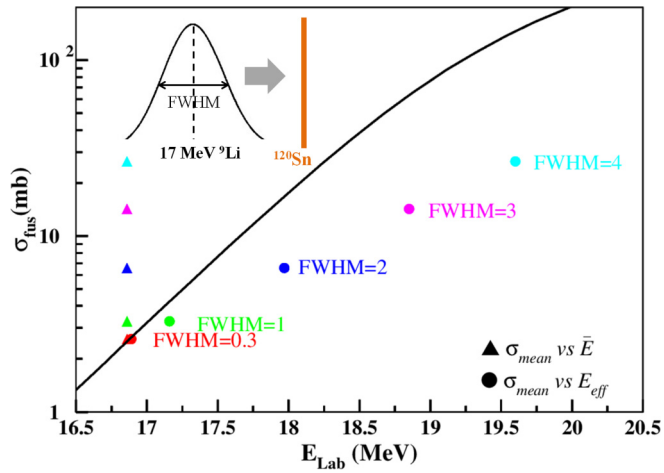

FIG. 12. (Color online) Results of simulations, for the $^{9}\text{Li} + ^{120}\text{Sn}$ system, considering beams having Gaussian energy distribution centered at 17 MeV but with different FWHM (which varies from 0.3 to 4 MeV), impinging on a thin ^{120}Sn (as sketched in the inset). The solid curve corresponds to the true cross-section used for the input to the calculation. The values of the σ_{mean} are plotted as either (σ_{mean}, $\bar{E}$) (triangles) or (σ_{mean}, E_{eff}) (circles). Each color represents different values of the FWHM.

could be claimed only for the point obtained for the narrower incoming energy distribution. All the other data points differ significantly from the true cross-section at 17 MeV.

As a further example, Fig. 13 shows a conceptually similar simulation to the one shown in Fig. 12 but relative to three different $D(E,t_0)$ distributions having similar FWHM but different shapes. As can be seen the presence of the high energy tail in the Gaussian-like distributions (labeled as A

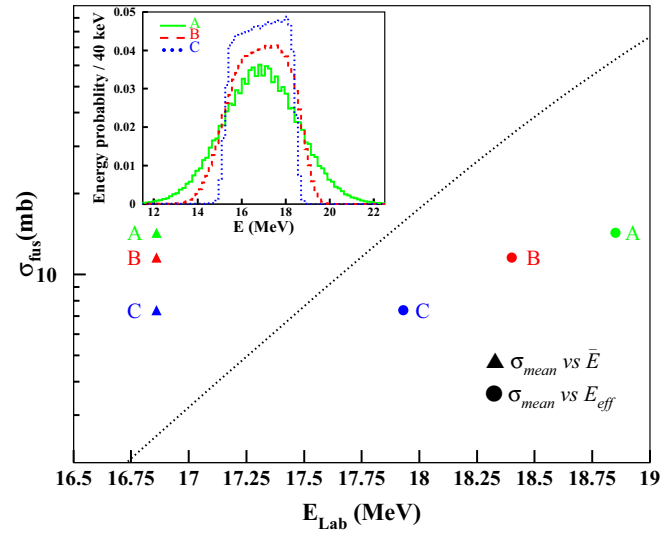

FIG. 13. (Color online) Results of simulations, for the $^{9}\text{Li} + ^{120}\text{Sn}$ system, relative to three different energy distribution inside a thin ^{120}Sn target having similar FWHM and different shapes (showed in the inset). The solid curve corresponds to the true cross-section used for the input to the calculation. The values of the mean cross-section σ_{mean} are plotted either as (σ_{mean}, $\bar{E}$) (triangles) or (σ_{mean}, E_{eff}) (circles).

and B) generates a non-negligible difference between the true curve and the inferred data points plotted either versus the mean energy or effective energy.

C. Consideration on previously published data

So far, different ingenious and difficult sub-barrier fusion experiments have been performed by different groups using RIBs (e.g., Refs. [10–12,14–18]). However, problems concerning energy straggling and foil nonuniformities are usually not explicitly reported. In the light of the present discussion, the reported fusion excitation functions might in some cases be affected by the problems presented in this paper since correctly measured mean cross-sections plotted versus $\bar{E}$ or $E_{\rm eff}$ might deviate from the real $\sigma_{\rm fus}(E)$ by non-negligible amounts. This subsection presents a short overview on some of the published fusion data measured with RIBs and the stack activation technique around the Coulomb barrier, trying to understand if the effects discussed in the present paper might play any role, and if enough experimental details are provided in the corresponding papers to evaluate such effects.

As a first example of the possible effects of the beam energy distribution, the ^{6}He + ^{206}Pb experimental fusion data of Ref. [15] have been considered, where a beam energy spread of 6 MeV FWHM is reported after the last target. The authors underline that the "energy spread distorts significantly the experimental data" [15]. To estimate the importance of the distortion effect they averaged a calculated excitation function with a Gaussian beam energy distribution of 3 MeV FWHM, concluding that, at the lowest measured energy, this effect "increases the cross-section by almost two orders of magnitude" [15]. The authors, however, do not unfold their experimental data which, therefore, are expected to deviate from the real fusion excitation function by orders of magnitude.

The ^{6}He + ^{206}Pb fusion has been measured again by a different group [18] using a beam having a Gaussian energy dispersion of 1.3 MeV FWHM after the last target and an average energy loss of about 0.5 MeV inside each of the four stacked targets. As qualitatively expected due to the lower beam energy spread, at a fixed $E_{\rm cm}$ energy the cross-section of Ref. [18] plotted versus $\bar{E}$ is about an order of magnitude lower than the one of Ref. [15]. As a final result of their study, the authors of Ref. [18] plot their measured cross-sections using a simplified effective energy approach, pointing out that without this correction "the cross-section become overestimated by a factor 3" [18]. However, as shown in the current paper, the effective energy based on the averaging procedure does not always lead to the correct excitation function. Therefore, the applied correction procedure for those previously published works should be reassessed. Moreover, the approach used in Ref. [18] does not take full account of all aspects of the energy loss inside the target. It is possible to demonstrate that Eq. (4) of Ref. [18] is related to Eq. (A10) of the current paper in the case of zero stopping power and small dependence of the straggling with energy.

Next the ^{6}He + ^{197}Au fusion data of Ref. [16] have been considered. For this experiment the typical beam energy spread associated with each measured cross-section below the Coulomb barrier is reported to be of the order of ±2.5 MeV (see Fig. 6 in Ref. [16]). In light of the effects previously discussed for the ^{6}He on ^{206}Pb with a beam energy spread of ± 3 MeV, non-negligible cross-section averaging effects, at the lowest measured energies, might be expected also in the Ref. [16] case. In order to evaluate the possible presence of such effects, the present authors fitted the ^{6}He + ^{197}Au fusion data of Ref. [16] with a monotonic curve which was conservatively assumed to be the actual fusion excitation function of the system. Then, using Eq. (14), the $\sigma_{\rm mean}$ values that would have been measured assuming a Gaussian energy distribution inside the target $D(E,t_0)$, with a FWHM = 5 MeV, were calculated. Results show that, in the center-of-mass energy range between 16 MeV and 18 MeV, the ratio $\sigma_{\rm mean}/\sigma(\bar{E})$ ranges from 2.5 to 1.5. This very conservative estimate suggests that fusion excitation function $\sigma(E)$ given in Fig. 10 of Ref. [16] is an overestimation of the real one in the lower beam energy range.

Similar estimates also have been undertaken for the ^{11}Be + ^{209}Bi data of Ref. [12], although the beam energy distribution is not reported in that paper. Assuming the use of uniform foils, we estimated that the width of $D(E,t_0)$ associated with the used experimental technique is about 3 MeV. In spite of the rather large $D(E,t_0)$, the estimated effects, obtained applying the deconvolution procedure discussed in Sec. II D are of the order of the reported error bars. This is due to the fact that these data are essentially above the barrier region, where $\sigma(E)$ is not very steep.

More recently, the ^{8}He + ^{197}Au fusion excitation function was measured down to the range of 1 mb with a postaccelerated ^{8}He beam of only 10^5 pps [17]. As stated in Ref. [17], "the target stacks consisted of two or three Au targets (6 mg/cm^2 thick), separated by Al foils (1 mg/cm^2 thick) to collect recoiling residues, and Al foils (from 2 to 10 mg/cm^2 thick) to degrade the beam energy." The different stacks were irradiated at energies of 2.34, 2.51, and 3.68 MeV/nucleon. Although some further information on the irradiated foil can be found in Ref. [31], unfortunately in the current paper, it is not explained which foils were irradiated at the different energies, and no information is given on foil uniformity or beam energy distribution. Therefore, in spite of the fact this was a difficult and innovative experiment, the problems discussed in this paper are not explicitly mentioned, and not enough information is given in the paper [17] to allow the reader to estimate such effects.

The overarching conclusion of these studies is the vital importance of characterizing target and degrader foils. This is especially true for experiments where steeply falling cross-sections below the Coulomb barrier are to be measured. Therefore the authors of the current paper strongly recommend that for future publications where such data are presented, enough information should be included concerning the composition of the target stacks; in particular, the target and degrader foils characteristics and their effects on beam energy distributions and on the extracted excitation functions. In this way others in the community can easily assess the accuracy of the results.

VI. STACKED TARGET EXPERIMENT WITH A STABLE BEAM

In order to further illuminate the nature of the experimental challenges, and how they may be addressed in an actual

experimental situation using stacked targets, the procedures discussed in this paper have been applied to the study of the fusion reaction ^{6}Li + ^{120}Sn. Since this is a stable beam reaction, and therefore a good quantity of data could be accumulated at low bombarding energy, it is not necessary to use thick targets. Nevertheless, it will be shown that, in spite of the use of a good quality stable beam and a stack made of only four relatively thin targets, the effects discussed in the present paper are still not negligible.

The ^{6}Li + ^{120}Sn fusion cross-section was measured at the Laboratori Nazionali del Sud by using a stacked target activation technique [32]. The yield of the ERs was determined by an off-line detection of the atomic x-rays emitted following their electron capture (EC) decay [9,13,14]. Two stacks made of four ^{120}Sn targets with an average thickness of 0.5 mg/cm^2, evaporated on ^{93}Nb catcher foils of 1.5 mg/cm^2, were irradiated by ^{6}Li beams, delivered by the Tandem Van de Graaff, at $E_{\rm lab} = 25$ MeV and at $E_{\rm lab} = 21$ MeV, respectively. From this data mean cross-section $\sigma_{\rm mean}$ were deduced. The targets were characterized by determining their surface morphology as reported in Sec. IV A. From this information the $D(E,t_0)$ functions for each target in the stack could be determined and the corresponding values of $\bar{E}$ and $E_{\rm eff}$ could be calculated. The data points are shown in Fig. 14: The open circles correspond to $(\sigma_{\rm mean},\bar{E})$, and the closed circles correspond to $(\sigma_{\rm mean},E_{\rm eff})$. So it can be seen that even if the average target thicknesses are thin, the difference in $\bar{E}$ and $E_{\rm eff}$ values is not negligible. It is interesting to observe that, as discussed in Sec. II C, in the case of uniform targets it is expected that the $E_{\rm eff}$ energy is always shifted toward higher values with respect to $\bar{E}$ because of the weighted average with the exponential increasing cross-section. Instead, in the presence of target nonuniformities the prediction of this shift is not straightforward. In fact, the presence of nonuniformities

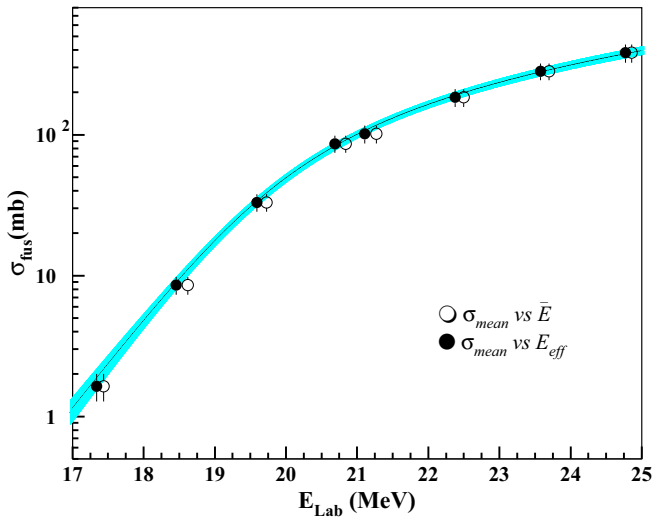

FIG. 14. (Color online) ^{6}Li + ^{120}Sn fusion excitation function. The open and closed symbols are the measured values of the fusion cross-section plotted versus $\bar{E}$ and $E_{\rm eff}$. The continuous black line shows the result of deconvolution procedure, discussed in Sec. II D; the blue shaded area represents the uncertainty associated with the procedure.

reduces the average interaction energy and its effect is to lower the effective energy. The final value of $E_{\rm eff}$ is a combination of these two effects. In the present case $E_{\rm eff}$ is always smaller than $\bar{E}$, but it has to be noticed that this shift differs from target to target, since it depends on the relative weight of the two effects, which is specific and unique for each target. In the same figure, the result of the deconvolution procedure, discussed in Sec. II D and applied to the present data, is also reported. As a starting *guess function*, for the deconvolution method, the following formula was used:

$$\sigma(E) = AE\ln[1 + e^{B(E-C)}]. \tag{16}$$

The parameters A, B, and C were varied in order to achieve the best fit as discussed in Sec. II D. The corresponding parameters are $A = 1.98 \pm 0.37$ mb MeV^{-1}, $B = 1.41 \pm 0.14$ MeV^{-1}, and $C = 19.37 \pm 0.24$ MeV. The blue shaded part represents the uncertainty in the result of the deconvolution procedure. The deconvolution curve is in good agreement with the fusion cross-section data plotted against the effective energy (closed circles), as one could expect, since the targets for this experiment are quite thin. The fusion cross-section data plotted against the mean energy (open circles) are systematically shifted towards higher energies. It is important to remark that, although in the present case the discussed effects are relatively small, in the typical experimental conditions involving RIBs such effects can be extremely important as shown in previous sections.

Before closing this subsection on the treatment of an actual experimental data set, it is important to emphasize that the use of energy loss codes plays a crucial role in any of the discussed procedures. It is important to bear in mind that, in general, there could be non-negligible differences in energy loss calculations performed by different codes. This can generate potential problems in all data analysis procedures based on energy loss calculations, as discussed, for example, in Ref. [33] for the case of resonant elastic scattering experiments. Results of energy loss calculations should always be critically cross checked and effects of possible uncertainties estimated.

VII. SUMMARY AND CONCLUSIONS

With the advent of new radioactive ion beam facilities, either commissioned or under construction, the exploratory potential for investigating nuclear processes to the outer limits of nuclear existence is an exciting emerging area of modern nuclear physics. But such new facilities bring challenges both for the production of RIBs and the experimental facilities to exploit these beams. In particular experimental techniques need to evolve in order to compensate for the inherent low intensity of these beams.

It has been shown in this paper that the stacked target technique can be used to great advantage when investigating nuclear reactions involving RIBs. But, for this old technique to be successfully used to produce measurable yields with these beams, multiple thick targets may often be needed. Due to the large number of stack foils, and/or their nonuniformities, and/or the quality of RIBs used, in many reported experiments in the literature targets have been irradiated by beams having rather large energy dispersion. Therefore, associating a

measured average cross-sections with the correct energy is not a trivial task. Some authors have simply used the mean energy of Eq. (2); others have used the effective energy of Eq. (3). However, this paper clearly shows that, in general, neither of these two methods is well founded. Indeed, when the energy distribution within a target is large, and the cross-section is rapidly changing with the energy, these approaches can lead to significant misinterpretations of the data. From this it would seem that the use of thick target stacks to investigate nuclear processes with RIBs is somewhat compromised. However, it is shown in this paper that accurate information still can be obtained in such circumstances provided accurate target characterization is undertaken. In such a way, every target is then assigned a $D(E,t_0)$ function, which specifies how the cross-section will be integrated over the RIB energy. It is recommended that the best procedure to infer the true excitation function is to deconvolute the experimental yields with the known $D(E,t_0)$ function convoluted with a prior-Bayesian cross-section function. So, in summary, providing certain precautions are observed, the stacked target technique can evolve into a very useful experimental tool for reaction studies of radioactive ion beams. However, for the reasons discussed in this paper, the present authors strongly recommend that for future publications where such data are presented, information should be included concerning the beam, targets, and degrader foils characteristics, together with statements of how these characteristics have influenced the data analysis and error propagation.

ACKNOWLEDGMENTS

The authors thank A. Del Zoppo, A. Vitturi, and A. Caciolli for useful discussions and suggestions. A.C.S. acknowledges with gratitude INFN for travel and subsistence support during this work. The authors from Catania acknowledge the partial financial support of the Italian Ministry of Education and Research (PRIN 2010-2011, Project No. 2010TPSCSP).

APPENDIX

In this appendix a simplified case will be considered to show analytically how $\bar{E}$ and $E_{\rm eff}$ deviate from the energy E_r, at which the measured mean cross-section $\sigma_{\rm mean}$ corresponds to $\sigma_{\rm mean} = \sigma(E_r)$.

Consider a Gaussian incoming beam energy distribution given by $e^{[-(E-E_0)^2/(2\mu_0^2)]}$, where E is the actual energy, E_0 the mean energy, and μ_0 is the standard deviation of the energy distribution, which interacts with a uniform target of thickness t_0. Due to energy losses, the beam will decrease its mean energy and increase its energy spread as it traverses the target. Suppose this decrease in mean energy is specified by a simple linear relationship:

$$E_m = E_0 - \beta t, \tag{A1}$$

where E_0 is the entrance energy, E_m is the mean beam energy after penetrating a distance t into the target, and β is a constant. The actual normalized energy distribution at depth t into the target will be given by:

$$\frac{e^{-\frac{(E-E_0+\beta t)^2}{2\mu_t^2}}}{\mu_t\sqrt{2\pi}}, \tag{A2}$$

where μ_t is the standard deviation of the energy distribution at target depth t, which will increase as the beam penetrates the target. As a first order assumption it is assumed that it varies as

$$\mu_t^2 = \mu_0^2 + at/2, \tag{A3}$$

where a is a constant. Suppose now that the reaction cross-section that is producing the radioactive nuclei of interest is given by:

$$\sigma(E) = \sigma_0 e^{-\alpha(E_0-E)}, \tag{A4}$$

where σ_0 is the cross-section at the entrance energy E_0 and α is taken as a constant. Such exponentially decreasing cross-sections are typical of fusion reaction processes below the Coulomb barrier.

The yield, Y, of the product nuclei for the target is therefore:

$$Y = \frac{N_{t_0}N_B}{t_0}\int_0^{t_0}\int_E \frac{\sigma_0 e^{-\alpha(E_0-E)}e^{-\frac{(E-E_0+\beta t)^2}{2\mu_t^2}}}{\mu_t\sqrt{2\pi}}dEdt, \tag{A5}$$

where N_{t_0} is the number of atoms per unit area of the target and N_B is the number of beam particles incident on the target. An average cross-section then can be assigned to this yield:

$$\sigma_{\rm mean} = \frac{Y}{N_{t_0}N_B}. \tag{A6}$$

To determine the actual energy E_r corresponding to this deduced mean cross-section, the expression for $\sigma_{\rm mean}$ Eq. (A6) can be substituted into the true cross-section relationship of Eq. (A4). The result is

$$E_r = E_0 + \frac{\alpha\mu_0^2}{2} + \frac{ln\frac{1-e^{-\gamma}}{\gamma}}{\alpha}, \tag{A7}$$

where $\gamma = \alpha t_0(\beta - a\alpha/4)$. The value of the mean energy $\bar{E}$ of the beam in the target is given by the following equation:

$$\bar{E} = E_0 - \frac{t_0\beta}{2}. \tag{A8}$$

The value of $E_{\rm eff}$ defined by Eq. (3) can be obtained by the following expression:

$$E_{\rm eff} = \frac{\int_0^{t_0}\frac{1}{\mu_t}\int_E E\sigma_0 e^{-\alpha(E_0-E)}e^{-\frac{(E-E_0+\beta t)^2}{2\mu_t^2}}dEdt}{\int_0^{t_0}\frac{1}{\mu_t}\int_E \sigma_0 e^{-\alpha(E_0-E)}e^{-\frac{(E-E_0+\beta t)^2}{2\mu_t^2}}dEdt}. \tag{A9}$$

The effective energy, $E_{\rm eff}$, defined by Eq. (3), and given by Eq. (A9), becomes:

$$E_{\rm eff} = E_0 + \alpha\mu_0^2 - \frac{[1-(1+\gamma)e^{-\gamma}]\left(\frac{1}{\alpha} - \frac{a}{4\beta-a\alpha}\right)}{1-e^{-\gamma}}. \tag{A10}$$

The question then arises as to whether the data point ($\sigma_{\rm mean}$, $E_{\rm eff}$) is actually a point on the true curve $\sigma(E)$. Clearly, by comparing Eqs. (A8) and (A10) with respect to Eq. (A7), one can see that both $\bar{E}$ and $E_{\rm eff}$ differ from the real expected

value of the energy E_r, and so the data points $(\sigma_{\text{mean}}, E_{\text{eff}})$ or $(\sigma_{\text{mean}}, \bar{E})$ do not lie on the true curve $\sigma(E)$.

For an immediate visualization of this important result, for the case where the $a = 0$ (i.e., assuming an energy spread constant within the target) in Eq. (A3), $\bar{E}$, E_{eff}, and E_r have been plotted in Fig. 2 as function of the energy loss in the target. This means that for each particular value of the target thickness t the respective energy distribution will have always the same width (i.e., $\mu_t = \mu_0$). The slope α of the exponential trend of the cross-section defined in Eq. (A4) has been chosen equal to $1.72\,\text{MeV}^{-1}$ (see Appendix for details). As it has been concluded in Sec. II C, $\bar{E}$ and E_{eff} can be considered a proper approximation of E_r only in the case of a monoenergetic beam and very thin targets.

[1] L. Canto, P. Gomes, R. Donangelo, and M. Hussein, Phys. Rep. **424**, 1 (2006).

[2] N. Keeley, R. Raabe, N. Alamanos, and J. Sida, Prog. Part. Nucl. Phys. **59**, 579 (2007).

[3] N. Keeley, N. Alamanos, K. Kemper, and K. Rusek, Prog. Part. Nucl. Phys. **63**, 396 (2009).

[4] A. Di Pietro, V. Scuderi, A. M. Moro, L. Acosta, F. Amorini, M. J. G. Borge, P. Figuera, M. Fisichella, L. M. Fraile, J. Gomez-Camacho, H. Jeppesen, M. Lattuada, I. Martel, M. Milin, A. Musumarra, M. Papa, M. G. Pellegriti, F. Perez-Bernal, R. Raabe, G. Randisi, F. Rizzo, G. Scalia, O. Tengblad, D. Torresi, A. M. Vidal, D. Voulot, F. Wenander, and M. Zadro, Phys. Rev. C **85**, 054607 (2012).

[5] M. Cubero, J. P. Fernández-García, M. Rodríguez-Gallardo, L. Acosta, M. Alcorta, M. A. G. Alvarez, M. J. G. Borge, L. Buchmann, C. A. Diget, H. A. Falou, B. R. Fulton, H. O. U. Fynbo, D. Galaviz, J. Gómez-Camacho, R. Kanungo, J. A. Lay, M. Madurga, I. Martel, A. M. Moro, I. Mukha, T. Nilsson, A. M. Sánchez-Benítez, A. Shotter, O. Tengblad, and P. Walden, Phys. Rev. Lett. **109**, 262701 (2012).

[6] A. Diaz-Torres and I. J. Thompson, Phys. Rev. C **65**, 024606 (2002).

[7] M. Dasgupta, P. R. S. Gomes, D. J. Hinde, S. B. Moraes, R. M. Anjos, A. C. Berriman, R. D. Butt, N. Carlin, J. Lubian, C. R. Morton, J. O. Newton, and A. Szanto de Toledo, Phys. Rev. C **70**, 024606 (2004).

[8] L. Canto, P. Gomes, J. Lubian, L. Chamon, and E. Crema, Nucl. Phys. A **821**, 51 (2009).

[9] A. Di Pietro, P. Figuera, E. Strano, M. Fisichella, O. Goryunov, M. Lattuada, C. Maiolino, C. Marchetta, M. Milin, A. Musumarra, V. Ostashko, M. G. Pellegriti, V. Privitera, G. Randisi, L. Romano, D. Santonocito, V. Scuderi, D. Torresi, and M. Zadro, Phys. Rev. C **87**, 064614 (2013).

[10] J. J. Kolata, V. Guimarães, D. Peterson, P. Santi, R. White-Stevens, P. A. DeYoung, G. F. Peaslee, B. Hughey, B. Atalla, M. Kern, P. L. Jolivette, J. A. Zimmerman, M. Y. Lee, F. D. Becchetti, E. F. Aguilera, E. Martinez-Quiroz, and J. D. Hinnefeld, Phys. Rev. Lett. **81**, 4580 (1998).

[11] P. A. DeYoung, B. Hughey, P. L. Jolivette, G. F. Peaslee, J. J. Kolata, V. Guimarães, D. Peterson, P. Santi, H. C. Griffin, J. A. Zimmerman, and J. D. Hinnefeld, Phys. Rev. C **58**, 3442 (1998).

[12] C. Signorini, A. Yoshida, Y. Watanabe, D. Pierroutsakou, L. Stroe, T. Fukuda, M. Mazzocco, N. Fukuda, Y. Mizoi, M. Ishihara, H. Sakurai, A. Diaz-Torres, and K. Hagino, Nucl. Phys. A **735**, 329 (2004).

[13] A. Di Pietro, P. Figuera, F. Amorini, C. Angulo, G. Cardella, S. Cherubini, T. Davinson, D. Leanza, J. Lu, H. Mahmud, M. Milin, A. Musumarra, A. Ninane, M. Papa, M. G. Pellegriti, R. Raabe, F. Rizzo, C. Ruiz, A. C. Shotter, N. Soić, S. Tudisco, and L. Weissman, Phys. Rev. C **69**, 044613 (2004).

[14] V. Scuderi, A. Di Pietro, P. Figuera, M. Fisichella, F. Amorini, C. Angulo, G. Cardella, E. Casarejos, M. Lattuada, M. Milin, A. Musumarra, M. Papa, M. G. Pellegriti, R. Raabe, F. Rizzo, N. Skukan, D. Torresi, and M. Zadro, Phys. Rev. C **84**, 064604 (2011).

[15] Y. E. Penionzhkevich, V. I. Zagrebaev, S. M. Lukyanov, and R. Kalpakchieva, Phys. Rev. Lett. **96**, 162701 (2006).

[16] Y. Penionzhkevich, R. Astabatyan, N. Demekhina, G. Gulbekian, R. Kalpakchieva, A. Kulko, S. Lukyanov, E. Markaryan, V. Maslov, Y. Muzychka, Y. Oganessian, R. Revenko, N. Skobelev, Y. Sobolev, D. A. Testov, and T. Zholdybaev, Eur. Phys. J. A **31**, 185 (2007).

[17] A. Lemasson, A. Shrivastava, A. Navin, M. Rejmund, N. Keeley, V. Zelevinsky, S. Bhattacharyya, A. Chatterjee, G. de France, B. Jacquot, V. Nanal, R. G. Pillay, R. Raabe, and C. Schmitt, Phys. Rev. Lett. **103**, 232701 (2009).

[18] R. Wolski, I. Martel, Ł. Standyło, L. Acosta, J. L. Aguado, C. Angulo, R. Berjillos, J. P. Bolivar, J. A. Duenas, M. S. Golovkov, T. Keutgen, M. Mazzocco, A. Padilla, A. M. Sánchez-Benítez, C. Signorini, M. Romoli, and K. Rusek, Eur. Phys. J. A **47**, 111 (2011).

[19] A. Lemut, Eur. Phys. J. A **36**, 233 (2008).

[20] N. Jovancevic, L. Daraban, and S. Oberstedt, Nucl. Instrum. Methods Phys. A **739**, 68 (2014).

[21] J. F. Ziegler, M. Ziegler, and J. Biersack, Nucl. Instrum. Methods Phys. B **268**, 1818 (2010)..

[22] J. Ziegler, "SRIM code" [http://www.srim.org].

[23] J. M. K. Tu and M. L. C. Feldman, *Electronic Materials Thin Film Science* (Macmillan, New York, 1992).

[24] L. Feldman and J. Mayer, *Fundamentals of Surface and Thin Film Analysis* (North Holland-Elsevier, New York, 1986).

[25] L. F. T. L. Alford and J. Mayer, *Fundamentals of Nanoscale Film Analysis* (Springer, Berlin, 2007)

[26] K. Seshan, *Handbook of Thin Film Deposition* (Elsevier, Amsterdam, 2002).

[27] *Thin Film Processes II*, edited by J. L. Vossen and W. Kern, (Academic Press, New York, 1991).

[28] C. Y. Wong, Phys. Rev. Lett. **31**, 766 (1973).

[29] P. Bevington and D. Robinson, *Data Reduction and Error Analysis for the Physical Science*, 3rd ed. (Mc Graw-Hill, New York, 2003).

[30] F. James and M. Roos, Comput. Phys. Commun. **10**, 343 (1975).

[31] A. Lemasson, Fusion et réactions directes autour de la barrière Coulombienne avec le noyau riche en neutrons ^{8}He, Ph.D. thesis, Universite de Caen (2010).

[32] M. Fisichella, A. C. Shotter, A. Di Pietro, P. Figuera, M. Lattuada, C. Marchetta, A. Musumarra, M. G. Pellegriti, C. Ruiz, V. Scuderi, E. Strano, D. Torresi, and M. Zadro, Eur. Phys. J. Web Conf. **66**, 03027 (2014).

[33] M. Zadro, A. D. Pietro, P. Figuera, M. Fisichella, M. Lattuada, A. Maggio, F. Pansini, M. Papa, V. Scuderi, O. Goryunov, and V. Ostashko, Nucl. Instrum. Methods Phys. B **259**, 836 (2007).